Electron Dynamics in Metallic Nanoparticles

M. Aeschlimann

Department of Physics, University of Kaiserslautern
Erwin-Schroedinger-Str. 46, D-67663 Kaiserslautern
Phone: +49-631-205-2322, Fax: +49-631-205-3903
e-mail: ma@physik.uni-kl.de

Excitation and relaxation of the conduction band electrons in metallic nanoparticles are discussed in the light of the results of line width measurements and femtosecond pump-probe experiments. The optical response is interpreted in terms of the particle (Mie-) plasmon resonance. The different mechanisms, which can lead to phase destruction as well as energy dissipation of the collective electron motion are revealed and pioneering experiments in this new field are reviewed. Most of the reported results indicate a strong size effect on the plasmon damping process, but only minor size effects on the following steps of the energy relaxation which corresponds to the internal and external thermalization of the optically excited electronic system.

Table of contents

I. INTRODUCTION

Excitation and relaxation of electrons in metallic nanoparticles play a key role in a number of important physical phemomena including linear and nonlinear optical effects. The main motivation for the interest in these systems is related to the possibility of tailoring, to a considerable extent, their electrodynamical behavior on the basis of size and shape. Furthermore, by studying the temporal evolution of collective electronic excitations (e.g. after a laser excitation) on the time-scale from a few femtoseconds to several picoseconds, one can improve the knowledge about basic properties of the light-matter interaction in metallic nanoparticles.

A typical signature of the optical response of metallic nanoparticles is given by the presence of a local plasmon resonance (Mie-plasmon, see II.A) [1,2,3]. While the positions of the resonances of Mie-plasmon excitation as a function of particle size, shape and dielectrictric properties are well understood (as an overview, see [1]), the ultrafast dynamics of these collective electronic excitations have remained a highly interesting topic to be revealed in much greater detail. An essential issue is how rapidly the collective excitation lose their phase coherence. Further, one would like to investigate the mechanisms responsible for dephasing. After these dephasing processes, typical internal and external thermalization processes set in to distribute the energy of the excited quasiparticles (single excited *hot* electron) into the electron gas and nanoparticle lattice and finally to the nanoparticle-substrate complex.

With the advance of ultrashort pulsed laser systems, transient (nonthermal) electron distribution can now be created and probed. Compared to the time-scale of these laser pulses the long-lasting nonequilibrium situation offers the unique possibility of analyzing the interactions (energy exchange) between the different subsystems (electron gas, phonon system, substrate/matrix complex).

In this paper all different energy dissipation steps after an ultrashort laserpulse are described in a sequential approach. However, one should keep in mind that this is a straightforward view. All processes start at once, but they are finalized on different time scales. I.e. electron gas energy losses happen before the electron gas is fully thermalized. It is just the time-scale of the different energy exchange mechanisms which differs over several magnitudes (from 10 fs to 120 ps) which allows, with some exception, this simplified treatment.

It is also important to mention that all considerations discussed in this article are relevant for metallic nanoparticles larger than 10 Å. The metal is still considered as a three-dimensional system. When the size becomes smaller than 10 Å, the discrete nature of the electronic states (quantum effects) shows up [4,5,6,7]. Above that size the width of the discrete levels becomes comparable to or larger than the separation between them, e.g. the conduction band is quasicontinuous and the behavior of the nanoparticles tends to approach that of the bulk metal, presenting, however, some significant differences concerning the electrodynamic properties.

II. ADSORPTION OF LIGHT IN METALLIC NANOPARTICLES

A. General considerations

The optical properties of nano-structured systems have been extensively investigated in order to reveal their fundamental processes and to examine possible technological applications [1, 2]. Concerning the interaction of visible light with metals the conduction electrons are of central importance. As a useful approximation all electrons can be described collectively as a plasma with density N_e [8]. A collective excitation of the dense electron gas in a metal is called *plasmon*. In the most general case the term *plasmon* describes a longitudinally collective oscillation of the electron plasma relative to the crystal lattice. This excitation

consists of a coherent motion of a high number of electrons in contrast to those excitations in which the external perturbation acts on a single electron. In general, one has to distinguish between bulk, surface, and particle (Mie) plasmons.

The *bulk plasmon* denotes a collective excitation of the electron gas in the bulk of the metal, which propagates as a longitudinal charge density fluctuation at a resonance frequency [9]

$$\omega_{Pl} = \sqrt{\frac{N_e \cdot e^2}{\varepsilon_0 m}} \,. \qquad (1)$$

The quanta of these bulk plasmon possess an energy $\hbar\omega_{Pl}$ which is for most metals in the order of 10 eV - 15 eV for metals. Excitation of bulk plasmons with light is not possible due to the longitudinal nature of bulk plasmons.

At *surfaces* the mobility of the electrons in a plane parallel to the surface is high (quasi free electrons) whereas perpendicular to the surface the mobility is limited due to the border of the metal. This results in a reduced energy of the collective mode ω_{SP} regarding to the bulk value ω_{Pl} [1,10]:

$$\omega_{SP} = \frac{\omega_{Pl}}{\sqrt{2}} \qquad (2)$$

Because the phase velocity of surface plasmons is slower than that of a photon with the same energy, direct coupling of freely propagating light to an excitation of surface plasmons is forbidden in a smooth metal film. However, the coupling is possible by means of two well known methods [1]: 1) the grating coupling method invokes modification of the surface with a lattice structure which adds additional reciprocal lattice vectors to the initial wavevector of the light. 2) the attenuated total reflection method exploits the total internal reflection inside a

prism which is attached to the metal film. Surface plasmons have been extensively studied with different optical methods, mainly because of their extremely high sensitivity to interface structures and adsorbates [1, 11].

In *metal nano-particles* with sizes smaller than the wavelength of light as well as the optical penetration depth, all atoms in the particle can be collectively excited. Hence, collective electronic oscillations, the so-called Mie plasmons, can be excited by light and are therefore detectable as a pronounced optical resonance in the visible or UV parts of the spectrum [1, 12, 13]. The resonance frequency of the oscillation is determined by the dielectric properties of the metal and the surrounding medium, and by the particle size and shape. The collective oscillation can be interpreted as a displacement of the center of mass of all electrons in the particle against the positively charged background of the atomic cores. There is no propagation of a (longitudinal) charge density fluctuation, hence, a plasmon in a metallic nanoparticle has to be distinguished from a propagating surface plasmon, not often done in the literature. This collective charge oscillation causes a large resonant enhancement f of the local field inside and near the particle [14]. This resonance dominates the linear and nonlinear response of the materials. The particle-size dependence and host-matrix dependence of the absorption spectrum have been discussed in many systems with Mie scattering theory [15]. In general, these studies took into account two contributions to the dielectric function $\varepsilon(\omega)$, a Drude term $\varepsilon_{intra}(\omega)$ originating from free electrons and an interband term $\varepsilon_{inter}(\omega)$ reflecting the band-to-band transitions [16].

Considerable interest has been focused on silver nanoparticles as they exhibit a particularly strong size-dependent optical resonance in the visible spectral range (1.8 eV - 3 eV), i.e., at energies below the interband transition threshold (~ 4 eV). Consequently, the absorption cross-section in the visible region is dominated by the Drude term [17]. The contribution due

to interband transitions is negligible. Quite contrary, investigation on isolated copper and gold nanoparticles allows to study the influence due to the strong overlap between the Mie-plasmon resonance (~ 2.3 eV) and the interband (d → sp) transition at ~ 2.4 eV. Hence, both the intraband and interband optical processes are involved in the material response to a light excitation.

B. Plasmon decay time

The most important factor for the coherent interaction of light with nanoparticles is the dephasing time

$$T_2 = 2\hbar/\Gamma_{hom} \qquad (3)$$

where Γ_{hom} is the homogeneous linewidth of the plasmon resonance. This dephasing time T_2 corresponds to the time scale on which the decay of the coherent electron plasma oscillation (and hence the local-field enhancement) takes place, e.g. the time scale on which the electron oscillation preserves the memory of the optical phase of the excitation pulse. This dephasing time is essential because e.g. the enhancement factor f of the electric field near the particle surface due to the collective excitation is expected to be proportional to T_2 [2,18]. Please notice that many authors use the expression plasmon lifetime $\tau_{sp} = \hbar/\Gamma_{hom}$. According to Eq. (3), the plasmon lifetime τ_{sp} is related to dephasing time T_2 by $2\tau_{sp} = T_2$.

In recent years several line width measurements and time-resolved second and third harmonic generation autocorrelation measurements [for the technique, see e.g. 19, 20, 21] on metallic nanoparticles have been published, reporting a dephasing time of the Mie-plasmon excitation on the order of 4 fs - 20 fs. All experimental studies have been performed in the low-excitation regime, where the energy optically transferred to the system is too small to strongly perturb the nanoparticle. In the following different experimental techniques will be discussed

which allow to determine the dephasing time T_2. The different mechanisms, which can lead to this phase destruction of the collective electron motion are discussed in the next section.

First experimental knowledge on line width of metallic nanoparticles in a two-dimensional arrangement was gained for thermally evaporated ultrathin films, which show a broad distribution in particle size and shape [2]. By this randomness a strong inhomogeneous broadening of the absorption band results which is much broader than the resonance of a single individual particle. This inhomogeneous broadening is caused by variations in size, shape, surface structure, and environment of the individual particles within the cluster ensemble. Since the magnitude of the inhomogeneous broadening is not known quantitatively, the homogeneous width Γ_{hom} and, hence, the dephasing time T_2 cannot be extracted. The absorption spectra only provide a lower limit of T_2.

Craighead *et al.* reported the first extinction spectra of a lithographically produced regular two-dimensional array of identical metal nanoparticles [22]. In contrast to thermally evaporated ultrathin films, by nanofabrication the size and shape of particles can be designed and the distribution width of these parameters can be extremely narrowed.

The potential of nanodesigned optical films in order to study plasmon decay dynamics has also been nicely demonstrated by Gotschy *et al*. They deposited nearly identical, parallel oriented silver particles on a transparent ITO substrate by use of electron-beam lithography [23]. Figure 1 shows a SEM picture of a two-dimensional array of elliptic-shaped nearly identical, parallel oriented silver particles. As particle size and interparticle distances can be varied independently, this method allows to tailor the optical properties of single particles. In addition, elliptic-shaped metal nanoparticles show two different plasmon resonances which lie at different wavelengths for light polarized parallel to the short and long axes (see e.g. Fig. 7).

From the experimentally obtained line widths Gotschy *et al.* expected a plasmon decay time of a few femtoseconds.

Another way to overcome the problem of inhomogenous broadening due to variations in the size and shape is the spectroscopy of a single particle. Using SNOM spectroscopy, Klar *et al.* measured the homogeneous line shape of the plasmon resonance in single gold nanoparticles [18]. The measured linewidth varies around a value of 160 meV (see Fig. 2), which corresponds to a plasmon dephasing time T_2 of 8 fs. Besides the single-mode resonances, they also observed more complex line shapes caused by electromagnetic coupling between close-lying particles (see Fig. 2c).

Träger and co-workers applied an interesting novel technique where size and shape selectivity of the clusters was obtained by optical hole burning after deposition [24]. They used this technique to extract dephasing times of silver nanoparticles with radii smaller than 10nm, dimensions which are not accessible by lithographic techniques.

Spectral hole burning is a well-known technique in atomic, molecular, and solid-state physics. The achievement of the authors was to adopt the method for the specific needs in order to investigate T_2 in metallic nanoparticles. The idea of the method is as follows: First, nanoparticles with a broad size distribution are prepared on a transparent substrate. After measuring their optical absorption spectrum, the nanoparticles are irradiated with nanosecond laser pulses, the photon energy being located within the inhomogeneously broadened absorption profile. The fluence of the light is chosen such that the temperature increase of the particles induced by rapid conversion of the absorbed energy into heat is sufficiently high to stimulate evaporation of atoms. As a result, the distribution changes and a hole is permanently burned into the absorption profile. Finally, the optical spectrum is measured a second time and subtracted from the spectrum of the particles as grown to determine the width of the hole,

i.e. Γ_{hom}. From the experimental results and a theoretical model of hole burning the linewidth of 260 meV corresponding to a decay time of 4.8 fs was extracted for silver nanoparticles with a radius of 7.5 nm. This T_2 value is at least a factor 2 smaller than one would expect from the bulk dielectric function of silver. The authors concluded that additional damping mechanisms, in particular surface scattering, come into play in this size regime.

A further way to obtain accurate decay time constants is by means of time- instead of frequency-resolved measurements. In principle, all fs real-time measurements use a two-pulse (pump-probe) technique: The first laser pulse drives the systems and the second, suitable delayed, probes the actual state. Lamprecht *et al.* fabricated noncentrosymmetric particles in order to study the decay time of particle plasmons by means of a real time second-order nonlinear optical (SHG) autocorrelation experiment [25]. SHG can be considered as an optimal noninvasive probe of plasmon dynamics, but a shape without centrosymmetry is an essential condition for high SHG efficiency. Fig. 3 shows an interferometric autocorrelation measurement (thin line) for gold nanoparticles. Also shown is the autocorrelation function of the laser pulse (bold line) measured with a nonlinear crystal (BBO). For gold the experiment revealed a dephasing time T_2 of 12 fs. In the case of silver the experimentally obtained values T_2 vary between 14 fs and 20 fs.

Using the same time-resolved SHG technique, Rubahn and co-workers studied the plasmon lifetime of Na nanoparticles with mean radii of $5 < r_0 < 55$ nm [26]. They found a pronounced maximum in T_2 of 20 fs (τ_{sp} = 10 fs) for nanoparticles of an average radius of 22 nm, with lifetimes decreasing both for smaller and for larger particle radii (see Fig. 4).

The major drawback of the real-time SHG method, the restriction to noncentrosymmetric particle shapes, can be eliminated by using third harmonic generation (THG). Lamprecht *et*

al. used this technique to study the decay of resonant and slightly off-resonant driven plasmons in gold nanoparticles [27]. By comparing the measured third order interferometric autocorrelation function of the plasmon field with a simulation based on a simple harmonic oscillator model, they obtained the same dephasing time T_2 of 12 fs in both (resonant and off-resonant) cases. For off-resonant excitation, the results show that the phase difference between the driving laser field and the driven plasmon oscillation is no longer constant at $\pi/2$ as in the resonant case but varies with time (beating, see Fig. 5).

C. Mechanisms for damping of a collective resonance in a metallic nanoparticle

While the dephasing time T_2 of metallic particles as a function of particle size, shape, and dielectric properties are well investigated, the physical mechanism responsible for dephasing has remained a highly interesting and debated topic. Knowledge of the dephasing mechanisms is essential for basic science and for a large variety of applications. Depending on the size, size distribution, shape, dielectric constant of the surrounding medium etc., the following potential mechanisms are: First, the plasmon can dephase by internal decay, e.g. a decay of the fixed phase correlation between the individual electronic excitations of the whole oscillator ensemble, described by the *pure dephasing time* T_2*. A typical mechanism is the decay of the collective mode due to inhomogeneous phase velocities caused by the spread of the excitation energy or the local inhomogeneity of the nanoparticles. The plasmon can also decay due to a transfer of energy into quasi-particles (electron-hole pairs, i.e. due to surface scattering, phonon scattering or e-e-scattering) or reemission of photons (radiation damping and luminescence [28, 29, 30, 31], described by T_1. The total dephasing of the plasmon is given by:

$$\frac{1}{T_2} = \frac{1}{2T_1} + \frac{1}{T_2^*}. \qquad (4)$$

In general it is predicted that for sizes below about 10nm surface scattering is quite essential [1, 24]. For larger particles, however, radiation damping become more pronounced. According to Liebsch [17], the overall broadening $\Gamma(\omega)$ due to Drude damping γ and radiation losses is given by the function

$$\Gamma(\omega) = \gamma + \omega B(\omega)/A_i. \tag{5}$$

The term B(ω) characterizes radiation damping and is given by

$$B(\omega) = \frac{4\pi^2 V}{3\ \lambda^3}, \tag{6}$$

where λ is the wavelength of the laser pulse and V the volume of an isolated metallic particle. A_i represent the depolarization factors. For an ideal spheroid, the A_i satisfies the same rule $A_1 + A_2 + A_3 = 1$, in the case of a sphere, $A_i = 1/3$. The Drude damping γ includes all microscopic damping processes due to photons, phonons, impurities, surface scattering, and electron-electron interactions. Compared with Drude damping the radiation damping is explicitly frequency dependent. In particular, this implies that the damping near the maximum of the plasmon resonance is not representative for the damping far from resonance. Below the resonance, radiation damping is weaker than at resonance, while above the resonance, it becomes rapidly stronger (see Fig. 6).

This theoretical prediction has been experimentally verified by Scharte *et al.* [17]. They used elliptically shaped metal nanoparticles with semi-axes of 40 nm by 80 nm and a height of 45 nm. Elliptic-shaped metal nanoparticles show two different plasmon resonances which lie at different wavelengths for light polarized parallel to the short (b) and long (a) axes, respectively (see Fig. 7). Tuning the laser wavelength to one of these two resonances allows to distinguish between resonance excitation and off-resonance excitation by simply changing the polarization of the laser pulse. In both cases the excitation is the result of an intraband process, since the excitation energies of the Mie-plasmons in those silver nanoparticles lie

below the interband transition threshold (~ 4 eV). Consequently, the absorption cross-section in the visible region is dominated by Drude damping. The contribution due to interband transitions is negligible.

Liebsch's theory predicts that collective plasma oscillations within the nano-particles are subject to the same microscopic Drude damping processes due to phonons, impurities, electron-electron interactions as off-resonance excitations [17]. None of these inelastic scattering mechanisms is reduced or absent if the electrons oscillate near the resonance excitation. The plasma mode signifies a larger amplitude of oscillation but not the presence or absence of a particular microscopic scattering mechanism.

However, as pointed out above, radiation damping is strongly laser wavelength dependent (see Eq. 5) which leads to a different damping along the axes of the ellipsoid as shown in Fig. 5. At first sight on Fig 7 it is surprising that both two different resonances in the extinction spectrum at ω_a = 2.1 eV and ω_b = 2.95 eV exhibit about the same FWHM, i.e. about the same Γ. However, as evident from Eq. (5), the radiation damping scales inversely with the depolarization factor A_i, i.e. the damping is also determined by these coefficients. Thus, for the low (high) frequency Mie plasmon, both $\omega B(\omega)$ and A are small (or large), so that $\Gamma_a(\omega) \approx \Gamma_b(\omega)$.

An interesting question arises concerning the lifetime of the plasma oscillation in the nano-particle near resonance and off resonance. The experimental method used to investigate the dynamical parameter T_1 and T_2 of optically excited electrons in a metal is the time-resolved two-photon photoemission (TR-2PPE). This method is known to be a highly accurate method to determine the dynamics of hot electrons in unoccupied and occupied states. The pump-probe technique enables a direct measurement of the dynamical properties in the time domain

with a resolution in the range of few femtoseconds [32, 33, 34]. The principle is schematically shown in Figure 8. A pump pulse excites electrons out of the valence band into usually unoccupied states (on or off a plasmon resonance) with energies between the Fermi and vacuum level. A second probe pulse subsequently photoemits the excited electrons. The photoemission yield depends on the transient population of these intermediate states as a function of the temporal delay of the probe pulse with respect to the pump pulse. The measured pump-probe-signal contains information on the energy relaxation time T_1 of the population in the intermediate state, as well as its dephasing time T_2.

In Figure 9 the FWHM derived from the autocorrelation 2PPE traces are plotted as a function of the state of polarization relative to the short axis (b). For comparison, the behavior of polycrystalline tantalum is also shown. The FWHM for tantalum is not affected by rotating the polarization angle of the incoming light. Therefore, any effect caused by an increase of the dispersion due to rotation of the half wave plate can be excluded. For the elliptical Ag-nanoparticles, however, a rotation of 90° reduces the FWHM from almost 75 fs in the 'b' direction (short-axis mode, resonant plasmon excitation) to 69 fs in the 'a' direction (long-axis mode, off-resonant plasmon excitation). Further rotation of the polarization to the short axis 'b' restores the long lifetime of the plasmon excitation. One should be aware that these FWHM values still include the autocorrelation of the laser pulse width. The autocorrelation traces of tantalum were measured at an intermediate state energy $E - E_F = 2.8$ eV. In this energy range, the lifetime of excited electrons in a transition metal is in the order of 1 fs and hence, the traces obtained for tantalum represent the pure laser autocorrelation curve. Any increase in the FWHM in the autocorrelation measurement for Ag nanoparticles compared to the Ta values must be caused by a lifetime effect of the optically excited electron system.

According to Eq. (5), the different damping rates obtained under on- and off-resonance conditions can also be explained by different magnitudes of radiation damping along the short and long axis of the elliptical particles, as shown in Figure 6. The increase in the FWHM of the TR-2PPE autocorrelation curve in Figure 9 is about a factor 2 smaller for the long-axis mode as compared to the short-axis mode, taking into account that the FWHM of the Ta measurements represents the FWHM of the laser autocorrelation curve. This trend agrees well with the theoretical calculation as shown in Fig. 6. For a light polarization along the short *b* axis, we would expect to observe a damping given approximately by $\Gamma_b = \Gamma_b(\omega_b)$. If we now rotate the polarization direction towards the long *a* axis without changing the laser frequency, we excite the high-frequency tail of the ω_a plasma mode (see Fig. 6) and expect to find the damping $\Gamma_a = (\omega_b)$, which is about twice as large as Γ_b.

It might be tempting to conclude from the FWHM results of Figure 9 that on-resonance collective excitations in general have a longer lifetime than excitations far from resonance. This is not correct, however, since the exact opposite should be obtained, if we perform the analogous experiment near the frequency ω_a a of the long-axis mode: For a polarization along the *a* axis, we observe this mode on resonance with a damping given by $\Gamma_a = \Gamma_a(\omega_a)$. If we rotate the polarization towards the short *b* axis, while keeping the laser frequency fixed at ω_a, we should observe a strong decrease in damping, since excitations of the nanoparticle along the short axis are less subject to radiation losses. Thus, in this alternative configuration, the collective mode ω_a detected on resonance has a shorter lifetime than the excitations in the low-frequency tail of the ω_b mode. To test this theoretical prediction it would be desirable to repeat the two-photon photoemission measurement with about 2.1 eV pump laser frequency.

On the basis of the above theoretical analysis we can give the following tentative interpretation of the observed two-photon photoemission spectra: The initial pump pulse excites an electron from an occupied state 1 to an intermediate state 2. The effective field governing this excitation consists of a superposition of external field and induced field generated by the dynamical response of the electrons of the Ag particle. Accordingly, the amplitude of this excitation process is greatly enhanced if the laser frequency coincides with the Mie resonance. Because of the strong intrinsic broadening of the Mie plasmon the induced contribution to the effective electromagnetic field exciting state 1 is coherent over rather short times of the order of 0.6 to 6 fs, corresponding to $\Gamma \approx 0.1$ - 1.0 eV (see Fig. 6). Since the energy of the intermediate state is about 2 eV above the Fermi energy, the excited electrons scatter quasi-elastically via phonons and impurities and inelastically via electron-electron processes, giving a typical overall lifetime of about 6 to 10 fs, corresponding to an imaginary part of the Ag quasi-particle self-energy of about 0.06 to 0.1 eV [33]. The probe beam excites the electron from the intermediate state to the final state 3 above the vacuum level such that it can be detected as an emitted electron. The probability of the second excitation process is also greatly enhanced if the probe laser is in resonance with the Mie plasma frequency. The probe pulse is subject to the same frequency-dependent damping mechanisms as the pump pulse. The measurements discussed in the present work suggest that time-resolved two-photon photoemission is sensitive not only to the decay of the intermediate electronic state but also to the intrinsic damping of the field enhancement causing the single-electron transitions.

Similar time-resolved 2PPE experiments have been performed by Lehmann *et al.* [35, 36]. They investigated the nonlinear response due to surface plasmons in silver nanoparticles on graphite. The results provide a direct evidence for multiplasmon excitation and allowed to identify two of their decay channels, namely, decay into one or several single-particle excitations.

III. DISSIPATION OF ENERGY (ELECTRONIC ENERGY RELAXATION)

A. Internal thermalization

As pointed out above, Drude and radiation damping are the dominant mechanisms for the decay of the collective excitation in a metallic nanoparticle with sizes > 10 nm. In the case of Drude damping the energy is transferred into one or several quasi-particle pairs (electron hole pairs). The next step of the energy relaxation corresponds to an *internal* thermalization of the electron gas. The excited electronic states tend to a Fermi-Dirac distribution with a well defined temperature which depends on the laser pulse intensity. The electron-electron scattering is the most efficient process to redistribute the energy to thermalize the electron gas. Quasielastic electron-phonon and electron-surface scattering do not play a dominant role in the dissipation of the excess energy of laser excited hot electrons, hence, no strong size effect in the thermalization process is expected. Also surface-plasmon-assisted resonant scattering of *d* holes into the conduction band as described by Bigot and co-workers is only relevant for sizes < 10 nm [37].

Fan and co-workers have shown in a time resolved photoemission experiment, performed in Au films, that the temporal scale of this thermalization process is of a few hundreds of femtoseconds [38]. No comparable direct measurement of the thermalization time has been reported so far for metallic nanoparticles. However, there are few indirect indications for a transient non-thermal component of the electron gas. Bigot *et al.* studied the non-thermal component in Ag nanoparticles (size 6.5 nm) embedded in a transparent matrix, using the pump-probe femtosecond spectroscopy [39]. Fig. 10 shows the differential transmission $\Delta T/T(t)$ excited with pulses of 30 fs duration at 800 nm, far from the plasmon resonance. The maximum of the signal is reached after a delay of $\approx$ 200 fs with respect to the laser pulse autocorrelation. This delay is a measure for the evolution from a nonthermal to a thermal

Fermi-Dirac distribution and is just slightly longer than the corresponding dynamics in silver film (delay ≈ 120 fs) as measured by Del Fatti *et al*. [40]. This indicates that the thermalization process due to electron-electron scattering is not much slower in metallic nanoparticles compared to a metal film in agreement with time-resolved two-photon photoionization measurements on free noble metal nanoparticles by Fierz *et al.* [41].

Similar electron dynamic studies in gold nanoparticles (size 22 nm) have been completed by Link *et al.* [42]. Taking into account that they used longer laser pulses (100 fs) the delay rise of the signal is in a good agreement with the results of Bigot *et al.* The authors modelled their results (decay of the bleach data) by a rate equation derived by Sun *et al.* [43]. The model consists of a modification of the two-temperature model (see below) including a nonthermal electron distribution part. From the obtained fitting parameter a thermalization time between 400 fs and 500 fs was obtained, in very good agreement with the values obtained by Sun *et al.* for 20 nm thin gold films.

Stella and co-workers also found a rise time in the transient reflectivity change in the order of 100 fs for tin nanoparticles embedded in an Al_2O_3 matrix [44]. They found that the build-up of the hot Fermi distribution was constant in the size range from 2 nm to 6 nm. It is expected that transition metals have a shorter thermalization time compared to noble metals, caused by the increased phase-space for electron-electron scattering due to the unfilled d-band.

It has to be noted, however, that the expression ‘thermalization time’ has never been deeply discussed so far, e.g. the question what fraction of electrons have to lie within the Fermi distribution until the electron gas can be called thermalized.

B. External thermalization: Energy transfer to the lattice

Let us now discuss the energy transfer from the hot electron system to the still cold lattice of the nanoparticles, often called external thermalization. In general it takes about a few ps until

a quasi-equilibrium state is formed between the electron system and the phonon system. This heat-exchange process is usually described by the electron-phonon coupling model developed for thin metallic films [45, 46, 47]. The electron system is characterized by an electron temperature Θ_e and the phonon system is characterized by a lattice temperature Θ_l, where each subsystem is assumed to be in local equilibrium. The time evolution of the temperatures are obtained with the heat equations [48, 49]:

$$C_e(\Theta_e)\frac{\partial \Theta_e}{\partial t} = -G(\Theta_e - \Theta_l) + p(t) \tag{8}$$

$$C_l \frac{\partial \Theta_l}{\partial t} = G(\Theta_e - \Theta_l) \tag{9}$$

where G reflects the *e-p* coupling constant, $C_e(\Theta_e)$ and C_l are electronic and lattice heat capacities, and $p(t)$ is the absorbed laser power density. The heat capacity of the electron gas is about two orders of magnitude smaller than the heat capacity of the lattice. Therefore, a high maximum electron gas temperature of several thousand Kelvins can be reached, although the rise of the equilibrium temperature is only a few hundred Kelvins [50].

In Eqs. 8 and 9 the electron energy losses are supposed to be proportional to the difference between the electron and lattice temperatures, the *e-p* coupling constant G governs the thermal equilibrium process. Due to the reduced dimensionality of the nanoparticles, however, the surface modes of the metallic particles will influence the energy transfer between the electrons and the lattice. Hence, a major goal in many studies has been to determine how the *e-p* coupling constant G changes as the particle size changes.

Most of the published results are obtained by means either of transient transmission and reflectivity measurements or transient absorption spectra as a function of the temporal delay between the pump and the probe beam. The increase in the electronic temperature induced by

the pump laser changes the real and imaginary part of the complex dielectric function $\varepsilon(\omega,t)$ of the particles, which causes transient changes in the spectrum (decrease in intensity, broadening and shift of the plasmon absorption band). The subsequent electron cooling via phonon emission results in a characteristic decay time τ of the modification of the optical constants. It has to be noted that the electronic heat capacity $C_e(\Theta_e)$ depends on the electron temperature Θ_e. Hence, the effective rate constant $\tau^{-1} = G/ C_e$ for the decay of the electronic temperature decreases as the initial electronic temperature increases; i.e., longer decay times are obtained for higher pump laser powers.

The response of the transient absorption spectra in respect to a nonthermal and thermal electron distribution at higher temperature can be modelled by combining the Mie equation with a theory developed by Rosei *et al.* [51].

Faulhaber *et al.* [52] measured the energy relaxation of gold particles (size 12 nm - 18 nm) by means of femtosecond absorption spectra and obtained a decay of about 7 ps, much larger than the decay on thin (d < optical penetration depth) gold films (τ < 2 ps, [45]). The authors explained the slower decay observed in nanoparticles that there is less non-equilibrium electron transport due to the spatial size confinement of the electrons in three dimensions.

In a gold nanoparticle system, Inouye and co-workers made white-light pump-probe experiments in the picosecond region, too [53]. They discussed the origin of the change in the transient differential absorption spectra for various delay times by decomposing the temporal behavior into two decay components, a fast component (< 3 ps) and a slow decay component (> 100ps). They suggested that the fast decay reflects the thermal equilibrium process between the electron system and the lattice system within the nanoparticles and the slow decay comes from the heat transfer between the nanoparticles and the host matrix as it will be discussed below. Quite contrary to the work of Faulhaber *et al.*, Inouye and co-workers

reported an *e-p* coupling constant *G* which was about two times larger than the result of a gold film [38, 45] indicating a faster decay in the particles.

The electron-phonon coupling time constant has also been investigated by Rubahn and co-workers for Na nanoparticles [26].They measured the relative change in the reflected second harmonic generation (SHG) signal of a pump-probe set-up. They obtained a decay of 1.1ps which is comparable to the values of for thin metal films [45], in opposite to the observation for gold nanoparticles by Inouye *et al.* [53] and Faulhaber *et al.* [52].

Also Hodak *et al.* found for Au (11 nm) and Ag (10 nm, 50 nm) nanoparticles similar relaxation times to those of bulk metals, which implies that there are no size-dependent effects in the heat-exchange between the electron and phonon system [54]. A similar result was obtained by Del Fatti *et al.* on Ag nanoparticles for the size range 3 nm $\leq$ R $\leq$ 13 nm [55]. Hence, one can assume that after a few tens of femtoseconds, the electrons have no memory of the way (intraband, interband, on or off Mie-resonance) they have been excited. Furthermore, Hodak *et al.* reported relaxation times which are strongly dependent on the pump laser power. This means that it is not possible to fit high-power (pump laser pulse) data using the simple two-temperature model calculations using a constant electronic heat capacity C_e in order to obtain *G*. They performed a series of measurements at successively lower pump laser powers and extrapolated the measured time constants τ to zero power. From the obtained data, the authors draw the conclusion that surface interaction have remarkably little effect on the electron-phonon coupling constant *G* for noble metal particles with diameter greater than 10 nm.

M. Nisoli *et al*. investigated the thermalization dynamics in gallium nanoparticles of different sizes in the solid and liquid phase [56]. They found clear size-dependent characteristic time

constants ($\tau \sim 0.6$ ps to 1.6 ps by increasing the size) but a quite similar temporal behavior of the electron energy relaxation in both phases (solid and liquid). In bulk the electron energy loss mechanisms are quite different in the two phases. These results shine some light on the role of the energy exchange with surface phonons in small metallic structures.

On the basis of all the published results one can summarize that the thermal equilibrium process between electron system and lattice system within the nanoparticles is larger than the internal thermalization time to a Fermi distribution, but still of the same magnitude. Hence, for a deeper theoretical treatment both processes have to be simultaneously included in the calculation. At present the reason for the rather different results for the electron-phonon coupling constant vs. size is not clear. One possibility for these discrepancies have been addressed by Bigot and co-workers [39]. They investigated the dynamics of Cu and Ag films in order to compare their behavior with the corresponding Cu and Ag nanoparticles, using the same experimental apparatus. The simultaneous measurement of the differential transmission and reflection as a function of the pump-probe delay allows to retrieve the time dependent complex dielectric function $\varepsilon(t)$ of the metal. Fig. 11 shows the normalized $\Delta\varepsilon_2$ and $-\Delta\varepsilon_1$ for the Cu film investigated for two probe wavelengths probed near and far from the interband optical transition. The curves show quite different relaxation times, especially the relaxation of the real part is much faster off resonance (0.4 ps) compared to on resonance (1.3 ps). The authors explained the differences due to the nonthermal character of the electron distribution after the pump laser pulse. This nonthermal population can persist for a long time near the Fermi level and has stronger effect on $-\Delta\varepsilon_1$. A similar effect was reported on Cu nanoparticles by the same authors. In Fig. 12 the time-dependence of $\Delta T/T$ decays with a longer relaxation time when the laser energy is at the plasmon resonance. One should keep in mind that, in the pump-probe experiment, the collective character of the electrons excited by the pump is lost within few tens of femtoseconds. Therefore, it is the plasmon that is created by the **probe**

which is sensitive to this mechanism. Hence, these effects have to be taken into account by comparing results of different groups obtained on the same metallic nanoparticles but at different wavelengths. This counts in particular for Cu and Au, for which the d → sp interband transition occurs at approximately the same frequency as the plasmon resonance. The situation is somehow simpler when the dynamics is studied far from the interband transition, e.g. for Ag where the interband transition is displaced to the plasmon resonance by > 0,7 eV.

Feldmann and co-workers investigated the vibrational dynamics of ellipsoidal silver nanoparticles after femtosecond laser pulse excitation [57]. They measured the differential transmission $\Delta T/T$ induced by a 150 fs laser pump pulse at $h\nu = 3.1$ eV and found the typical two-step decay (fast and slow decay) as discussed by Hodak *et al.*. In addition, the signals exhibit periodic modulations during the second decay step as shown in Fig. 13. The modulation periods are found to be independent of pump intensity, but show a strong dependence on the particle axis probed. They explained their results the following way: The heating by the pump pulse results in a thermal expansion of the particle. The electron pressure to this expansion is extremely large due to the high temperature of the electron gas. During this expansion, the inertia of the ions will make them overshoot their new (high-temperature) equilibrium positions. This overshoot will be followed by a reversal of the expansion, due to the elasticity of the metal, resulting in an oscillating behavior of the particle-length. These particle-length oscillations are expected to induce a plasmon shift which can even quantitatively explain the observed modulation in the differential transmission change $\Delta T/T$.

C. Heat transfer between the nanoparticles and the support

The last step in the energy relaxation is the heat transfer between the nanoparticles and the support (host matrix, substrate) which happens in a time scale above 100 ps. This process is sensitive to the thermal conductivity of the surrounding medium. In this time region we can consider that the lattice temperature of the nano-particles is the same as the electron temperature.

At first we can consider the thermal diffusion from the metallic nanoparticle to the substrate by a simple diffusion equation,

$$\frac{\partial \Theta_{subst}}{\partial t} = D_{subst} \nabla^2 \Theta_{subst}, \qquad (10)$$

where $D_{subst.}$ is the diffusivity of the heat in the substrate. From Eq. (10) we obtain the thermal distribution function outside of the metal nanoparticle as a function of the distance r and time t. In the case of a dielectric substrate, thermal diffusion inside the nano-particle can be neglected, because in general, diffusivity of metal, D_m, is 10^3 time larger than D_{diel}.

As already mentioned above, Inouye and co-workers found in a gold nanoparticle a slow decay component (~120 ps) and elucidated it as the heat transfer between the nanoparticles and the host matrix [53]. Also Hodak and co-workers found a slow component on a ~ 100 ps time scale in their transient bleach data recorded with a high-power (> 1 mJ/cm^2) pump laser for Au particles (10 nm) in a solvent [54]. For sufficiently high pump power, the heat deposited into the lattice by the electrons causes the particles to expand. This shifts the plasmon band to the red, leading to a long lived transient absorption and bleach signals on the red and blue sides of the plasmon band, respectively. For gold particles with a mean diameter of 30 nm in a sol-gel matrix, Perner *et al.* found a slow decay constant of 200 ps [58].

IV. CONCLUSION

The impact of ultrafast excitation and relaxation of the conduction band electrons of metallic nanoparticles have been reviewed. The attention is confined to metallic nanoparticles with sizes larger than 10 Å, e.g. the metal is still considered as a three-dimensional system. Quantum size effects due to the discrete nature of the electronic states [4] do not show up and do not play a role in the energy dissipation processes. However, the size of the nanoparticles is smaller than the wavelength of light as well as the optical penetration depth. Hence, all atoms in the particle can be collectively excited which influences the excitation (optical properties) and relaxation (electrodynamic properties) process.

Summarizing the general trend: Only the interaction of light with the nanoparticles shows a strong size dependency, especially the damping (dephasing time) and, hence, the resonant enhancement f of the local field depends critically on the size of the particles. But as soon as the energy is stored in the electron system (e.g. in electron-hole pairs), the following thermalization processes (electron cooling dynamics) show - if at all - only a slight size dependence. In addition, independent whether the light is absorbed due to plasmon absorption or interband transition, no difference is observed in the femtosecond electron dynamics as clearly shown by Link *et al.* [42].

So far most of the published work has been performed on noble metal nanoparticles, only few results were reported on transition metal particles. The detailed study of the electron dynamics in transition metal nanoparticles would help to understand the influence of the more localized d-band to the energy dissipation dynamics. Also from the point of catalytic reaction, the move to the more reactive transition metals would be desirable.

Furthermore, spin and time-resolved measurement open the possibility to study the spin-dependent electron dynamics in magnetic nanoparticles, a new research field which just has emerged in the last years [59, 60].

V. ACKNOWLEDGMENTS

The author would like to thank R. Porath, T. Ohms, M. Scharte, J. Beesley, M. Wessendorf, C. Wiemann, O. Andreyev, B. Lamprecht, H. Ditlbacher, J.R. Krenn, F. R. Aussenegg, A. Liebsch, J. Feldmann, H.-G. Rubahn, and J.-Y. Bigot for their contribution to many experimental results that are reported here. Special thanks go to M. Bauer and C. Ziegler for critical comments on various aspects of this manuscript. This work was supported by the Deutsche Forschungsgemeinschaft through SPP 1093.

Referees

[1] H. Raether, *Surface Plasmons*, Springer Tracts in Modern Physics, Vol. 111 (Springer, Berlin, 1988)

[2] U. Kreibig and M. Vollmer, *Optical Properties of Metal Clusters*, Springer Series in materials Science, Vol.25, (Springer, Berlin 1995)

[3] C. Bohren and D. Huffmann, *Absorption and Scattering of Light by Small Particles,* (John Wiley, New York, 1983)

[4] A. Bettac, L. Köller, V. Rank, K.H. Meiwes-Broer, Surf. Sci. **402-404**, 475 (1998)

[5] H.-V. Roy, P. Fayet, F. Patthey, W.-D. Schneider, B. Delley, and C. Massobrio, Phys. Rev. B **49**, 5611 (1994)

[6] G.K. Wertheim, S.B. DiCenzo, and D.N.E. Buchanan, Phys. Rev. B **33**, 5384 (1986)

[7] H. Handschuh, G. Ganteför, P.S. Bechthold, and W. Eberhardt, J. Chem. Phys. **100**, 7093 (1994)

[8] B. Lamprecht, Dissertation at the Karl-Franzen-University of Graz 2000, unpublished

[9] H. Raether, *Excitations of Plasmons and Interband Transitions by Electrons*, (Springer, Berlin 1980)

[10] D. Pines, Rev. Mod. Phys. **28**, 184 (1956)

[11] B. Lamprecht, J.R. Krenn, G. Schider, H. Ditlbacher, M. Salerno, N. Felidj, A. Leitner, F.R. Aussenegg, and J.C. Weeber, Appl. Phys. Lett. **79**, 51 (2001)

[12] G. Ritchie, E. Burstein, and R.B. Stephens, J. Opt. Soc. Am. B **2**, 544 (1985)

[13] M. Meier, A. Wokaun, and P.F. Liao, J. Opt. Soc. Am. B **2**, 931 (1985)

[14] H. Wenzel, H. Gerischer, Chem. Phys. Lett. **76**, 460 (1980)

[15] G. Mie, Ann. Phys. **25**, 377 (1905)

[16] B.R. Cooper, H. Ehrenreich, and H.R. Philipp, Phys. Rev. **138**, 494 (1965)

[17] M. Scharte, R. Porath, T. Ohms, and M. Aeschlimann, J. R. Krenn, H. Ditlbacher, F. R. Aussenegg, and A. Liebsch, Appl. Phys. B **73**, 305 (2001)

[18] T. Klar., M. Perner, S. Grosse, G. von Plessen, W. Spirkl, and J. Feldmann, Phys. Rev. Lett. **80**, 4249 (1998)

[19] J.-C.M. Diels, J.J. Fontaine, I.C. McMichael, and F. Simoni, Appl. Opt. **36**, 1270 (1985)

[20] C. Spielmann, L. Xu, and F. Krausz, Appl. Opt. **36**, 2523 (1997)

[21] D. Meshulach, Y. Barad, and Y. Silberberg, J. Opt. Soc. Am. B **14**, 2122 (1997)

[22] H.G. Craighead and G.A. Niklasson, Appl. Phys. Lett. **44**, 1134 (1984).

[23] W. Gotschy, K. Vonmetz, A. Leitner, F.R. Aussenegg, (1996), Opt. Lett. **21**, 1099 (1996)

[24] F. Stietz, J. Bosbach, T. Wenzel, T. Vartanyan, A. Goldmann, and F. Träger, Phys. Rev. Lett. **84**, 5644 (2000)

[25] B. Lamprecht, A. Leitner and F.R. Aussenegg, Appl. Phys. B, **68**, 419 (1999).

[26] J.-H. Klein-Wiele, P. Simon, and H.-G. Rubahn, Phys. Rev. Lett. **80**, 45 (1998)

[27] B. Lamprecht, J.R. Krenn, A. Leitner and F.R. Aussenegg, Phys. Rev. Lett. **83**, 4421 (1999)

[28] J.D. Jackson, *Klassische Elektrodynamik* (Walter de Gruyter, Berlin, New York, 1983)

[29] A. Wokaun, in *Solid State Physics*, H. Ehrenreich, T. Thurnbull, and F. Seitz, eds. (Academic, New York 1984), Vol **38**, p. 223

[30] F.J. Heilweil and R.M. Hochstrasser, J. Chem. Phys. **82**, 4762 (1985)

[31] M. Adelt, S.Nepijko, W. Drachsel, H.-J. Freund, Chem. Phys. Lett. **291**, 425 (1998)

[32] C.A . Schmuttenmaer, M. Aeschlimann, H.E. Elsayed-Ali, R.J.D. Miller, D. Mantell, J. Cao, and Y. Gao; Phys. Rev. B. **50**, 8957 (1994)

[33] M. Aeschlimann, M. Bauer, and S. Pawlik, Chem. Phys., **205**, 127 (1996)

[34] M. Wolf, Surf. Sci. **343**,377 (1997)

[35] J. Lehmann, M. Merschdorf, W. Pfeiffer, A. Thon, S. Voll, and G. Gerber, J. Chem. Phys. **112**, 5428 (2000)

[36] J. Lehmann, M. Merschdorf, W. Pfeiffer, A. Thon, S. Voll, and G. Gerber, Phys. Rev. Lett. **85**, 2921 (2000)

[37] T.V. Shahbazyan, I.E. Perakis, and J.-Y. Bigot, Phys. Rev. Lett. **81**, 3120 (1998)

[38] W.S. Fann, R. Storz, H.W. Tom, and J. Bokor; Phys. Rev. B **46** , 13592 (1992)

[39] J.-Y. Bigot, V.Halté, J.-C. Merle., A. Daunois, Chem. Phys. **251**, 181 (2000)

[40] N. del Fatti, R. Bouffanais, F. Vallée, and C. Flytzanis, Phys.Rev.Lett. **81**. 922 (1998)

[41] M. Fierz, K.Siegmann, M. Scharte, and M. Aeschlimann, Appl. Phys. B **68**, 415 (1999)

[42] S. Link, C. Burda, Z.L. Wang, and M.A. El-Sayed, J. of Chem. Phys. **111**, 1255 (1999)

[43] C.-K. Sun, F. Vallée, L.H. Acioli, E.P. Ippen, and J.G. Fujimoto, Phys.Rev.B. **50**, 15337 (1994)

[44] A. Stella, M. Nisoli, S. De Silvestri, O. Svelto, G. Lanzani, P. Cheyssac, and R. Kofmann, Phys. Rev. B. **53**, 15 497 (1996)

[45] H.E. Elsayed-Ali, T.B. Norris, M.A. Pessot, and G.A. Mourou, Phys. Rev. Lett. **58**, 1212 (1987).

[46] R.W. Schoenlein, W.Z. Lin, J.G. Fujimoto, and G.L. Eesley, Phys. Rev. Lett. **58**, 1680 (1987).

[47] C.-K. Sun, F. Vallée, L. Acioli, E.P. Ippen, and J.G. Fujimoto, Phys. Rev. B **48**, 12365 (1993).

[48] S.I. Anisimov, B.L. Kapeliovich, and T.L. Perel'man, Sov. Phys. JETP **39**, 375 (1974).

[49] G.L. Eesley, Phys. Rev. B **33**, 2144 (1986).

[50] S.A. Nepijko, S.A. Gorban, L.V. Viduta, and R.D. Fedorovich, Int. J. Electronics **73**, 1011 (1992)

[51] R. Rosei, F. Antongeli, and U.M. Grassano, Surf. Sci. **37**, 689 [1973)

[52] A.E. Faulhaber, B.A. Smith, J.K. Andersen, and J.Z. Zhang, Mol. Cryst. Liq. Cryst. **283**, 25 (1996)

[53] H. Inouye, K. Tanaka, I. Tanahashi, and K. Hirao, Phys. Rev. B **57**, 11 334 (1998)

[54] J.H. Hodak, I. Martini, and G.V. Hartland, J. Phys. Chem. B **102**, 6958 (1998).

[55] N. Del Fatti, F. Vallée, and C. Flytzanis, Y. Hamanaka, A. Nakamura, Chem. Phys. **251**, 215 (2000)

[56] M. Nisoli, S. Stagira, S. DeSilvestri, A. Stella, P. Tognini, P. Cheyssac, and R. Kofman, Phys. Rev. Lett. **78**, 3575 (1997).

[57] M. Perner, S. Gresillon, J. März, G. von Plessen, J. Feldmann, J. Porstendorfer, K.-J. Berg, and G. Berg, Phys. Rev. Lett. **85**, 792 (2000)

[58] M. Perner, P. Bost, U. Lemmer, G. von Plessen, J. Feldmann, U. Becker, M. Mennig, M. Schmitt, and H. Schmidt, Phys. Rev. Lett. **78**, 2192 (1997)

[59] U. Wiedwald, M. Spasova, M. Farle, M. Hilgendorff, and M. Giersig, J. Vac. Sci. Technol. **A 19**, 1773 (2001)

[60] F. Kronast, B. Heitkamp, H.A. Dürr, W. Eberhardt, G. Bihlmayer, S. Blügel, A. Liebsch, S. Landis, and B. Rodmacq, to be published

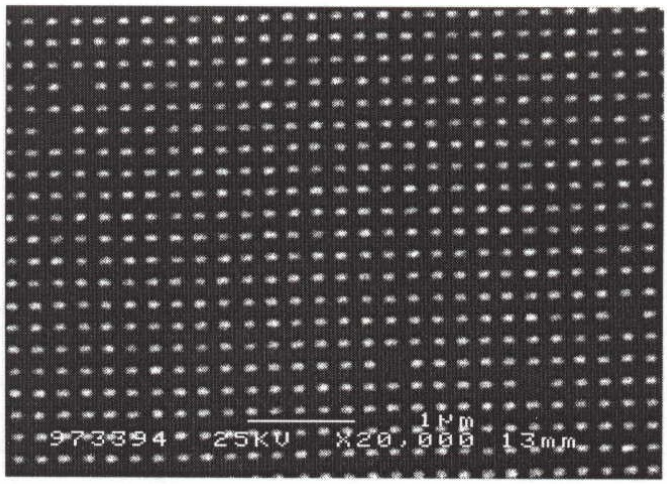

Figure 1: SEM picture of lithographically fabricated nanoparticles on ITO (Reprinted with permission from [23]).

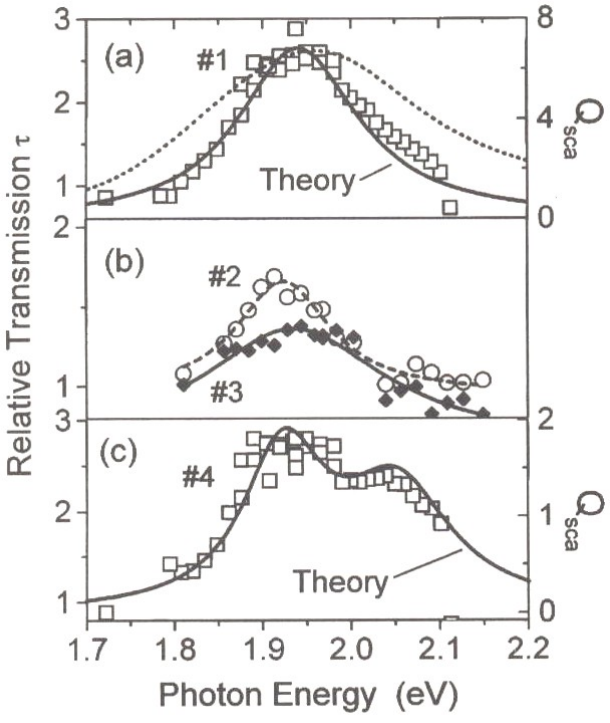

Figure 2: Near-filed transmission spectra of individual nanoparticles: (a) Particle #1 (squares); solid line: calculated Mie scattering efficiency Q_{sca} ; dotted line: far-field optical density of the composite film in arbitrary units. (b) Particles #2 (circles) and #3 (diamonds); dashed and solid lines: Lorentzian fits to the data. (c) Object #4; solid line: theory (Reprinted with permission from [18]).

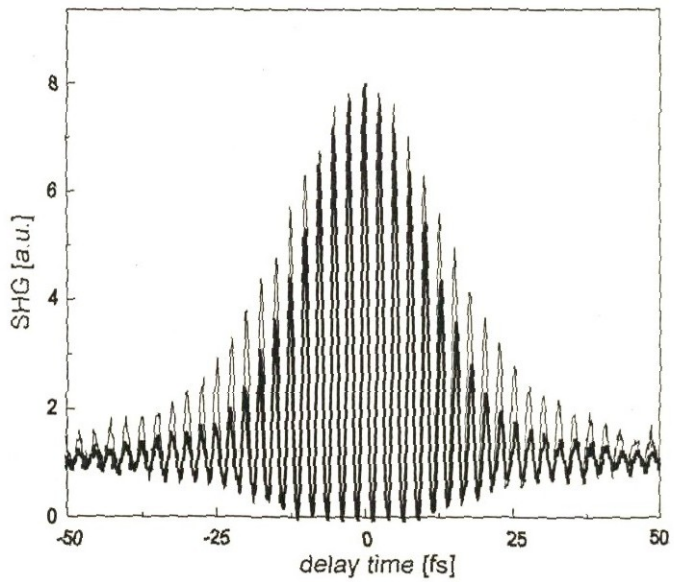

Figure 3: Interferometric autocorrelation functions for the laser pulse *(bold)* measured with BBO crystal and the SHG signal (thin line) for gold nanoparticles (Reprinted with permission from [25]).

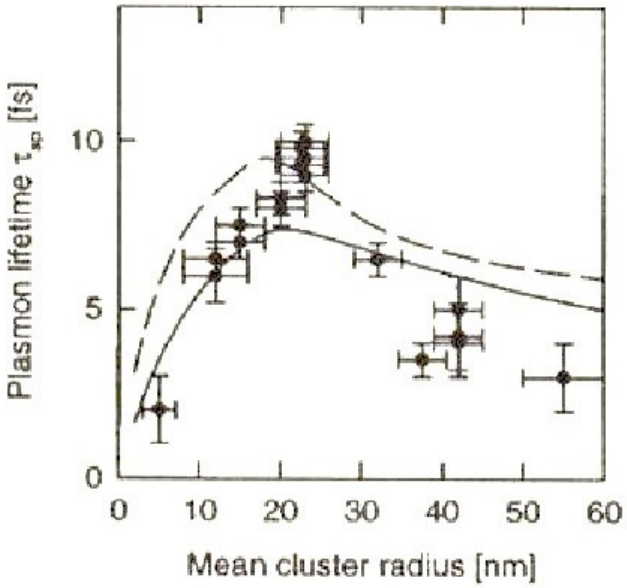

Figure 4: Measured plasmon lifetimes as a function of mean cluster radius for Na clusters adsorbed on mica. (Reprinted with permission from [26]).

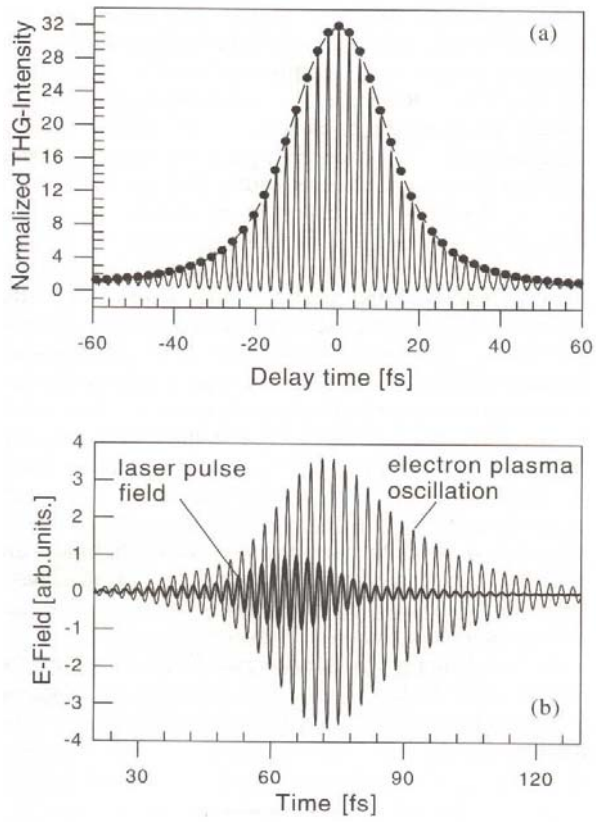

Figure 5: (a) Solid line: measured third order autocorrelation functions for an *off-resonantly* excited particle plasmon, maximum normalized to 32; filled circles: envelope of the calculated autocorrelation functions (the dashed line serves as a guide to the eye). (b) Driving laser pulse filed together with the calculated *off-resonant* plasmon field oscillation (Reprinted with permission from [27]).

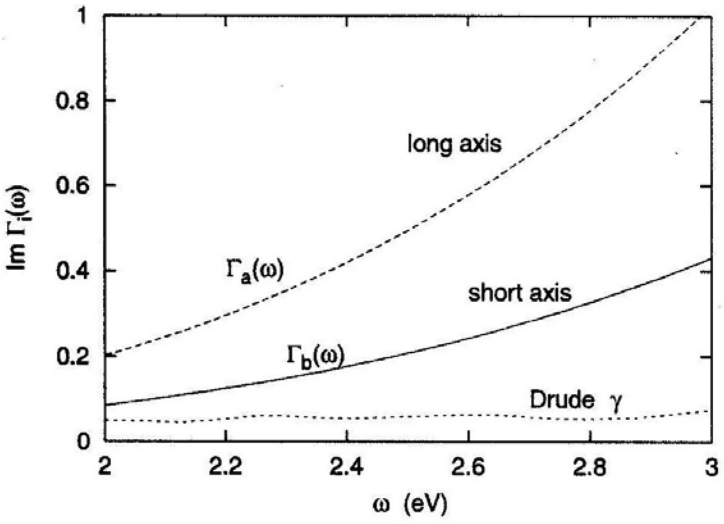

Figure 6: Plasmon broadening $\Gamma_i(\omega)$ as a function of frequency. *Solid curve:* damping of high-frequency mode $(\Gamma_b(\omega)$ (ω_b = 2.9 eV, short axis); *dashed curve:* damping of low-frequency mode $(\Gamma_a(\omega)$ (ω_a = 2.1 eV, long axis); *dot-dashed curve:* Drude damping γ derived from bulk optical data (Reprinted with permission from [17]).

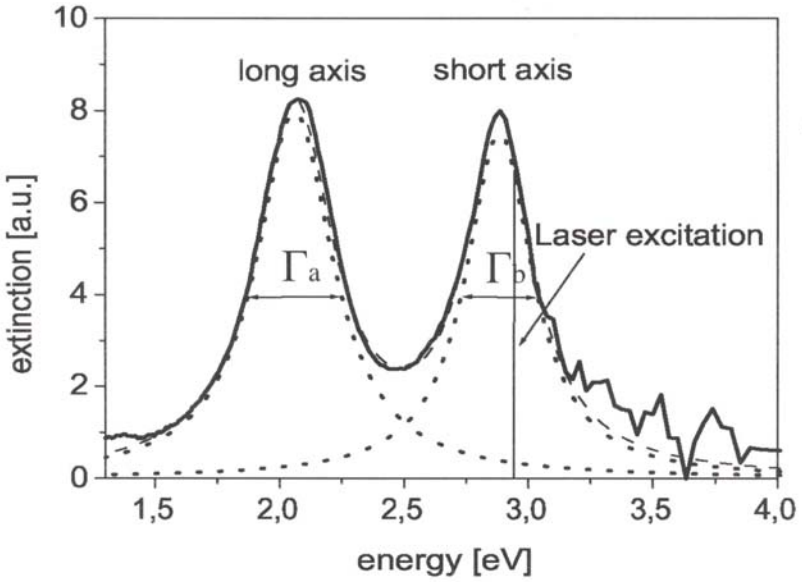

Figure 7: Measured extinction spectrum of the nanoparticle array. The low- and high-frequency peaks correspond to the Mie-plasmon, excited along the long and short axes of the elliptical Ag particles, respectively.

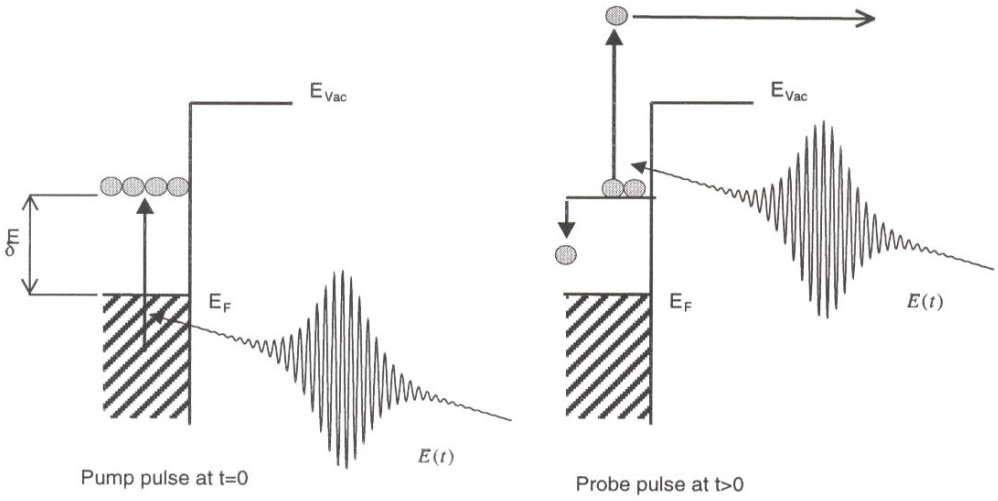

Figure 8: Principal mechanism of the time-resolved two-photon-photoemission (TR-2PPE) and the temporal behavior of the population N(t) in the intermediate state.

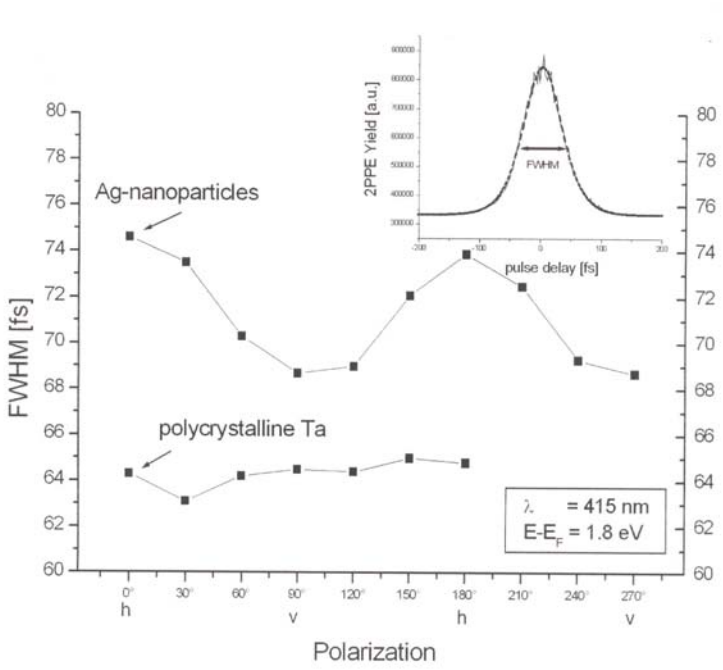

Figure 9: Nanoparticles show a variation of the FWHM of the autocorrelation over rotating states of polarization while tantalum shows no effect. In the inset a typical autocorrelation measurement can be seen from which the data points have been derived.

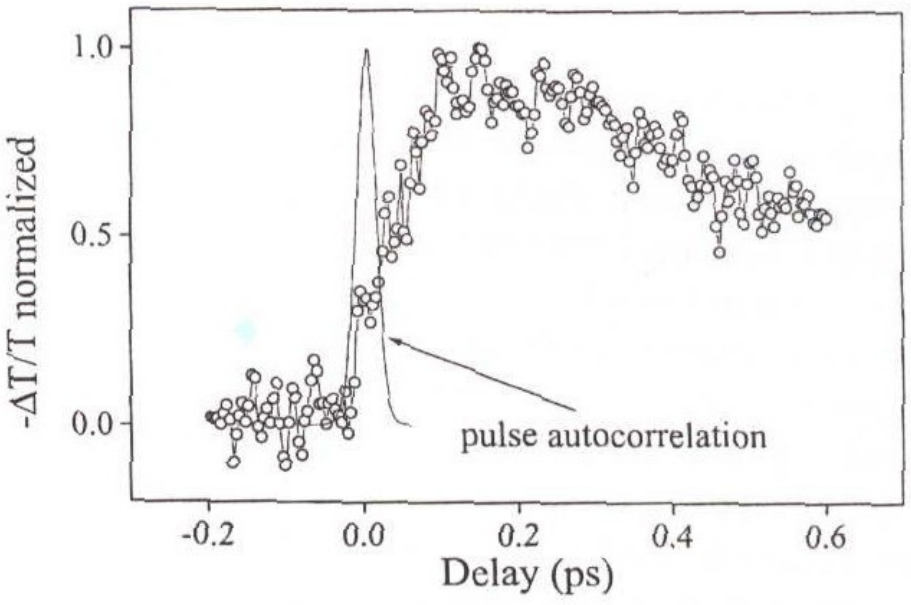

Figure 10: Differential transmission $\Delta T / T(t)$ of 6.5 nm Ag nanoparticles excited with pulses of 30 fs duration at 800 nm. The normalized pulse auto-correlation is shown as a reference (Reprinted with permission from [39]).

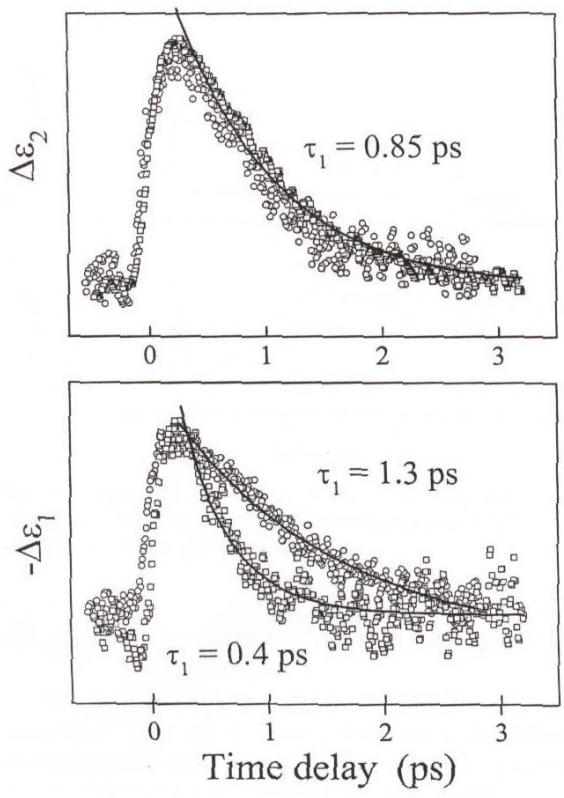

Figure 11: Dynamics of the normalized $\Delta\varepsilon_2$ and - $\Delta\varepsilon_1$ for the Cu film for two probe wavelengths near (circles: λ = 570 nm, 2.175 eV) and far (squares: λ = 611 nm, 2.03 eV) from the interband optical transition (Reprinted with permission from [39]).

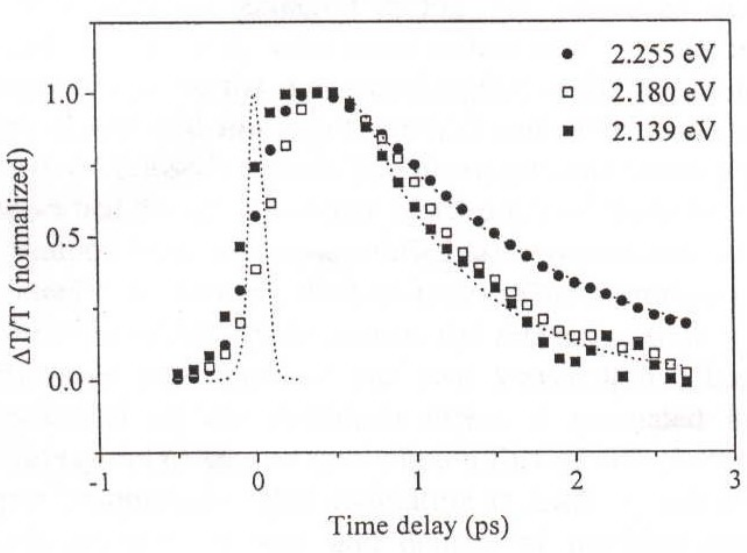

Figure 12: Time dependence of ΔT / T in Cu nanoparticles of 10 nm diameter in the vicinity of the surface plasmon resonance. The dotted line is the cross correlation between the 60 fs pump and 10 fs probe pulses (Reprinted with permission from [39]).

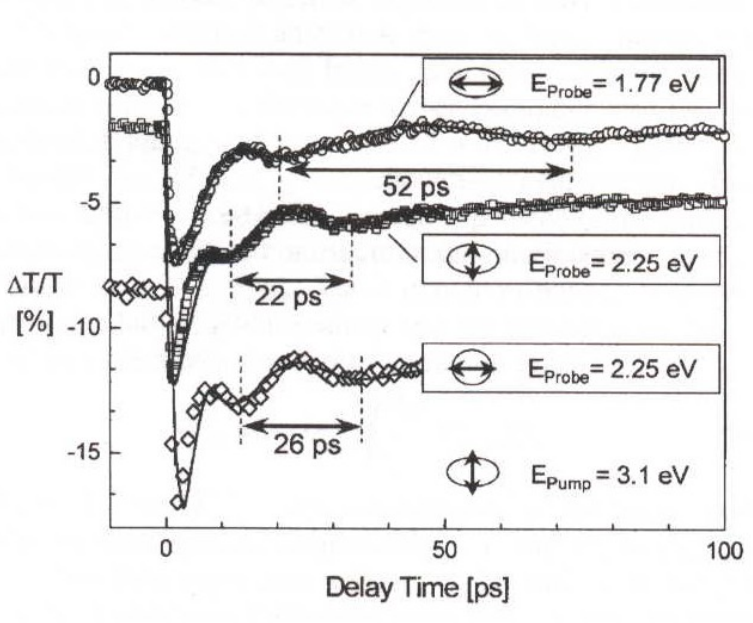

Figure 13: Differential transmission transients (upper curves: ellipsoidal particles; lowest curve: spherical particles; the transients are vertically offset for clarity). The light polarizations and photon energies of the pump and probe pulses are indicated. (Reprinted with permission from [57]).